IEEE Access
Multidisciplinary | Rapid Review | Open Access Journal

SPECIAL SECTION ON MISSION CRITICAL SENSORS AND SENSOR NETWORKS (MC-SSN)

Received November 29, 2018, accepted December 7, 2018, date of publication December 19, 2018, date of current version April 3, 2019.

Digital Object Identifier 10.1109/ACCESS.2018.2886825

Non-Contact Detection of Vital Signs Using a UWB Radar Sensor

ZHENZHEN DUAN, (Member, IEEE), AND JING LIANG, (Senior Member, IEEE)
Department of Information and Communication Engineering, University of Electronic Science and Technology of China, Chengdu 611731, China

Corresponding authors: Zhenzhen Duan (lollipopdzz@163.com) and Jing Liang (liangjing@uestc.edu.cn)

This work was supported in part by the National Natural Science Foundation of China under Grant 61671138 and Grant 61731006, and in part by the 111 Project B17008.

ABSTRACT The ultra-wide band (UWB) radar sensor is useful in the field of mission critical sensors and sensor networks due to its short detection time, high penetration, and low energy consumption. To support critical missions such as search and rescue, this paper designs a non-contact detection system based on a UWB radar sensor module to obtain vital signs of human beings. There are noise and clutter due to non-contact detection, and therefore the coherent background noise removal and moving target display filter are applied. Then, the variational mode decomposition (VMD) algorithm is used to extract heartbeat signals and respiratory signals. In addition, the Hilbert transform is applied to heartbeat signals and respiratory signals to obtain the time-frequency information. The electrocardiogram is also employed to compare the results of the UWB radar sensor. We also detect the human target through-the-wall. It turns out that the system can obtain respiratory and heartbeat characteristics simultaneously in one measurement, saving cost with high accuracy.

INDEX TERMS Mission critical sensors, non-contact detection, variational mode decomposition, electrocardiogram, through-the-wall detection.

I. INTRODUCTION

UWB signals' characteristic is that they do not need to adopt traditional carrier modulation in wireless transmission and reception, so it is convenient to process UWB signals in time domain [1]. The UWB radar sensor has advantages over other existing tools thanks to its high penetration, low power consumption and high-speed broadband [2]. It is effective to make through-the-wall measurements using UWB radar sensors due to its strong penetration ability [3]–[5]. UWB sensors can be widely applied in special patient monitoring, rescue after the earthquake and other fields due to its excellent features [6], [7].

Respiratory frequency is a very important physiological feature, and it is also an important diagnostic basis for doctors in clinical diagnosis [8]. The number of breaths per minute varies with age, gender, and physiological state. The detection of respiratory frequency can reflect some diseases. In clinical medical diagnosis, currently used respiratory detection devices are electrode-type chests impedance scanning method. When the respiratory detection device is working normally, a minute current flows through the body of the test subject [9]. ECG is a method commonly used to detect the characteristics of respiratory and heartbeat. The study of ECG detection signals is mainly the study of QRS characteristics [10]. Despite the high accuracy of ECG detection results, there are still some problems that need to be solved. The effective frequency of the ECG signal is within 0.67Hz to 40Hz [11]. It is not easy to detect by ECG when the patient's heart rate is too slow. What's more, when the device is used for a long period of time, there is a danger of the electrode pads sticking to the skin. This kind of device is also not suitable for patients with skin damage. Rational use of the advantages of UWB radar sensors can solve these problems. In the existing literature, Staderini of Tor Vergata University first proposed the non-contact monitoring of patients with UWB radar. The radar was placed on the bed and used to monitor the patient's breathing [12]. Igor Immoreev and Teh-Ho Tao applied the UWB radar sensor to non-contact patient monitoring and designed a detection system [13]. The system has been tested in the hospital in Moscow [14]. Reference [15] used the UWB radar sensor to measure the distance for the human target and detected respiratory characteristics. Zito *et al.* [16] developed a wearable respiration detection system. Its detection accuracy is close to

the contact type life monitor [17], [18]. Reference [19] conducted in-depth research on bio-radar detection of human life parameters. However, when the subject is breathing freely, the detection system cannot accurately detect the heartbeat signal. Traditional time-frequency analysis methods have almost all deficiencies. The UWB radar sensor can study frequency characteristics of various human motions [20].

However, these studies failed to detect both respiratory and heartbeat characteristics in the same test using UWB radar sensors. It is necessary to process echo signals with modal decomposition algorithms to obtain the characteristics of respiratory and heartbeat at the same time. The contributions of this paper are:

1. A detection system for the human body based on the UWB radar sensor is designed and original type omnidirectional dipole antennas are replaced with quasi Yagi antennas. The use of quasi Yagi antennas reduces the inherent antenna coupling noise.
2. Both respiratory and heartbeat motions are obtained from signals that have been preprocessed. respiratory and heartbeat can be acquired simultaneously by once detection. It saves time and cost. Moreover, there is a high accuracy of respiration detection. In addition, the time-frequency information got by the Hilbert transform verifies that using the VMD algorithm to process echo signals can effectively separate the respiratory and heartbeat motions.
3. We also conducted through-the-wall human respiratory detection so as to verify the wide-range applications of the system we designed.

The rest paper are organized as follows: Section II is the overall signals processing for human detection. It concludes three parts. Section III talks about the detection experiment and result analysis. The experiments contain detection without obstacle and detection through-the-wall.

II. SIGNALS PROCESSING FOR HUMAN DETECTION

The UWB radar sensor has strong penetration, so it is possible to directly measure the heartbeat vibration through the surface of the human body. The overall system block diagram based on the UWB radar sensor is shown in the FIGURE 1:

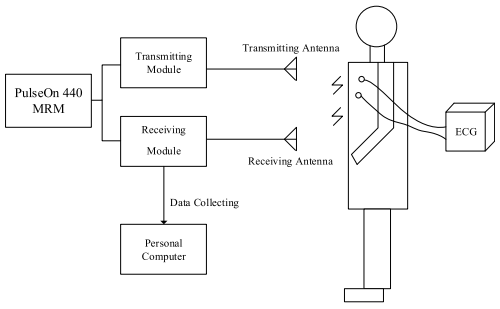

FIGURE 1. The overall system based on the UWB radar sensor.

Firstly, the human target faces the transceiver antennas, and keep the body as still as possible. Secondly, the UWB radar sensor system generates a series of UWB pulse signals and emits a first-order Gaussian pulse through the transmitting antenna. The thoracic motion causes the signals to be modulated in frequency and phase. Finally, the receiving antenna receives the echo signals and sends them to the computer for digital signal processing to extract the target's vital signs.

The digital signals processing flow chart is as the FIGURE 2.

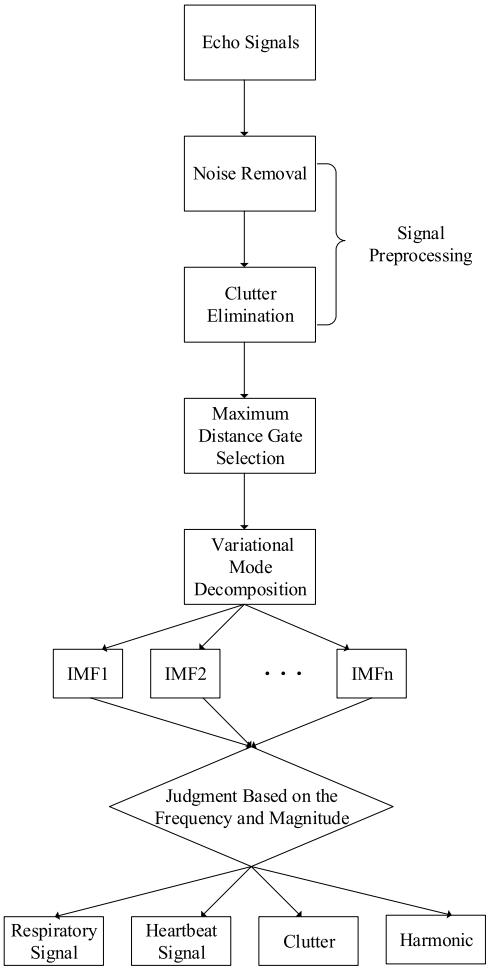

FIGURE 2. Digital signals processing for human detection.

Next, we will analyze and introduce the content of each part in detail.

A. ECHO SIGNALS PREPROCESSING

Because of the influence of the measuring environment and auxiliary equipments, the original echo signals are not ideal [21]. The signals detected by the UWB radar sensor need to be preprocessed. The preprocessing methods include coherent background noise removal and clutter filtering.

1) COHERENT BACKGROUND NOISE REMOVAL

The background noise of the measurement environment can be eliminated or reduced by using coherent background noise removal. Then, the effect of UWB radar sensor detection

can be improved. Collecting environmental detection echo signals A_b without human bodies firstly. Then, gathering echo signals A_o when the human body is present. Finally, we can get the human target echo signals A by deleting the scene information from the original echo signals(1). A is constructed from N scans and the length of each scan is M.

$$A = A_o - A_b \tag{1}$$

2) CLUTTER FILTERING

Generally speaking, signals of vital signs are weak because of the presence of background clutter. Background clutter usually consists of low frequency, DC components and some linear slowly changing trends. This paper uses moving target display filter to eliminate the constant part of signals. A_{diff} is a M by (N-1) matrix.

$$A = \begin{pmatrix} s_{11} & \cdots & s_{1n} \\ \vdots & \ddots & \vdots \\ s_{m1} & \cdots & s_{mn} \end{pmatrix} \tag{2}$$

$$A_{diff} = \begin{pmatrix} s_{11} - s_{12} & \cdots & s_{1(n-1)} - s_{1n} \\ \vdots & \ddots & \vdots \\ s_{m1} - s_{m2} & \cdots & s_{m(n-1)} - s_{mn} \end{pmatrix} \tag{3}$$

This method is simple and effective for clutter elimination.

Signals of vital signs are stronger than those without preprocessing. As shown in the FIGURE 3 and FIGURE 4, because of preprocessing methods, it is clear that the data is more concentrated. Noise is reduced using coherent background noise removal and clutter is filterd using MTI.

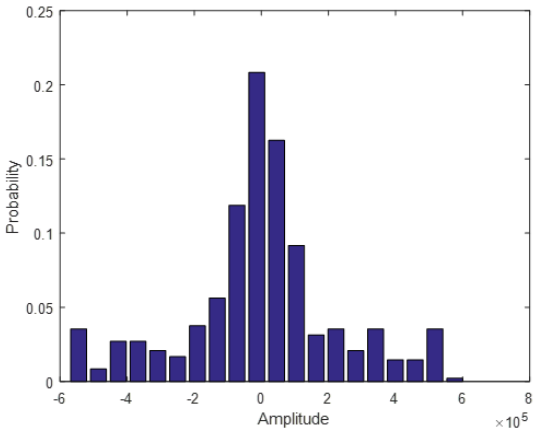

FIGURE 3. Raw echo data.

B. MAXIMUM DISTANCE GATE SELECTION

UWB radar sensor itself can measure distance based on tha time-of-arrival [22]. But we still use maximum distance gate selection because of the high precision measurement of respiratory and heartbeat information. Echo signals received by the receiving antenna are in the form of a two-dimensional matrix, which is M by N. M is the fast sampling number and N is the slow sampling number. Corresponding to the distance

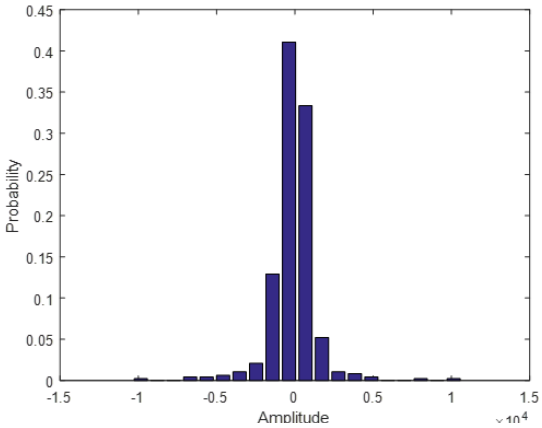

FIGURE 4. Preprocessed echo data.

information, follow the steps below to select the maximum distance gate:

1. Calculate the time delay $\Delta\tau$ based on the distance between the human body and the transceiver antennas:
$$\Delta\tau = \frac{2d}{c} \tag{4}$$
where d is the distance between the target and the antennas and c is the wave speed.
2. Select the maximum distance gate Δg according to the equation(5):
$$\Delta g = \frac{\Delta\tau}{\Delta t} \tag{5}$$
where Δt is represented by time index. Thus the equation(5) can be written as the equation(6):
$$\Delta g = \frac{2d}{c\Delta t} \tag{6}$$

C. VARIATIONAL MODE DECOMPOSITION

In order to acquire respiratory and heartbeat signs, the echo signals after preprocessing shuold be processed by mode decomposition algorithms. Although Discrete Fourier Transform can convert time domain signals into frequency domain signals [23], we still need a better algorithm to obtain weak information. Since VMD algorithm is suitable for nonstationary signals, it is appropriate for extracting respiratory and heartbeat signals.

The VMD algorithm is based on the steady mathematical theory. Two signals with similar frequency can be successfully separated by VMD algorithm [24]. VMD algorithm defines intrinsic mode functions(IMF) as the equation (7):

$$u_k(t) = A_k(t)\cos(\varphi_k(t)) \tag{7}$$

where $u_k(t)$ is the IMF and $\varphi_k(t)$ is the phase of it. The instantaneous frequency of $u_k(t)$ is $\omega_k(t)$, $\omega_k(t) = \frac{d\varphi_k(t)}{d(t)}$. $A_k(t)$ is the instantaneous amplitude of $u_k(t)$. For every $u_k(t)$, $A_k(t) \geq 0$, $\varphi_k(t) \geq 0$, $\omega_k(t) \geq 0$. The change velocities of envelope $A_k(t)$ and instantaneous frequency $\omega_k(t) = \frac{d\varphi_k(t)}{dt}$ are far less than those of phase $\varphi_k(t)$, so $u_k(t)$

can be regarded as a kind of harmonic signal whose amplitude is $A_k(t)$ and frequency is $\omega_k(t)$.

The steps of the VMD algorithm are constructing the variational problem and solving the variational problem.

Constructing the variational problem:

1. For each IMF $u_k(t)$, its analytic signal is calculated by Hilbert transform in order to obtain its unilateral spectrum.
$$\left(\delta(t)+\frac{j}{\pi t}\right)*u_k(t) \tag{8}$$
2. The analytical signals obtained in (8) are mixed with the respective center frequencies so that the respective spectra are shifted to the baseband.
$$\left[\left(\delta(t)+\frac{j}{\pi t}\right)*u_k(t)\right]e^{-j\omega_k t} \tag{9}$$
3. Calculate the L2 norm of the squared gradient of the demodulation signal obtained by equation (9) to estimate the bandwidth of each modal signal.
$$\min_{\{u_k\},\{\omega_k\}}\left\{\sum_k\left\|\partial_t\left[\left(\delta(t)+\frac{j}{\pi t}\right)*u_k(t)\right]e^{-j\omega_k t}\right\|^2\right\} \tag{10}$$
where $\{u_k(t)\}=\{u_1,\ldots,u_k\}$. $\{\omega_k\}$ is the corresponding center frequency. $\{\omega_k\}=\{\omega_1,\ldots,\omega_k\}$. $\sum_{k=1}^{K}$ is the sum of all intrinsic mode functions.

The variational problem is solved as in equation (11), shown at the bottom of this page, where α is the penalty coefficient. $\lambda(t)$ is the lagrangian multiplier. $s(t)$ is the echo signal.

The alternating directions method of multipliers(ADMM) is used to get the optimal solution of the (11). $\{u_k(t)\}$ can be represented as the equation (12), shown at the bottom of this page. Where ω_k is equivalent to ω_k^{n+1}. The equation (13),shown at the bottom of this page, is the frequency domain form of (12). Then, convert (13) into a form of non-negative frequency integral to get (14), shown at the bottom of this page. Thus the solution to the variational problem is as the equation (15), shown at the bottom of this page, and the center frequency ω_k^{n+1} is updated to the equation (16), shown at the bottom of this page.

Based on the alternating directions method, set preprocessed signals as $s(t)$. Follow the steps below to get IMF:

1. Initialization processing: $n=0$, $\{\hat{u}_k^1\}$, $\{\omega_k^1\}$, $\hat{\lambda}^1$.
2. For $n=n+1$, start iteration.
3. When k is in the interval $[1,K]$, update $\hat{u}_k$ and ω_k based on (15) and (16).
4. Update the lagrangian multiplier as the formula (17) shows. τ in (17) can be zero.
$$\hat{\lambda}^{n+1}(\omega)\leftarrow\hat{\lambda}^n(\omega)+\tau\left[\hat{s}(\omega)-\sum_k\hat{u}_k^{n+1}(\omega)\right] \tag{17}$$

Lagrange Expression.

$$L(\{u_k\},\{\omega_k\},\lambda)=\alpha\sum_k\left\|\partial_t\left[\left(\delta(t)+\frac{j}{\pi t}\right)*u_k(t)\right]e^{-j\omega_k t}\right\|^2+\left\|s(t)-\sum_k u_k(t)\right\|^2+\left\langle\lambda(t),s(t)-\sum_k u_k(t)\right\rangle \tag{11}$$

ADMM.

$$u_k^{n+1}=\arg min\left\{\alpha\left\|\partial_t\left[\left(\delta(t)+\frac{j}{\pi t}\right)*u_k(t)\right]e^{-j\omega_k t}\right\|^2+\left\|s(t)-\sum_k u_k(t)+\frac{\lambda(t)}{2}\right\|^2\right\} \tag{12}$$

$$\hat{u}_k^{n+1}=\arg\min\left\{\alpha\left\|j\omega\left[1+sgn(\omega+\omega_k)\cdot\hat{u}_k(\omega+\omega_k)\right]\right\|^2+\left\|\hat{s}(\omega)-\sum_k\hat{u}_k(\omega)+\frac{\hat{\lambda}(\omega)}{2}\right\|^2\right\} \tag{13}$$

$$\hat{u}_k^{n+1}=\arg\min\left\{\int_0^\infty 4\alpha(\omega-\omega_k)^2\left|\hat{u}_k(\omega)\right|^2+2\left|\hat{s}(\omega)-\sum_k\hat{u}_k(\omega)+\frac{\hat{\lambda}(\omega)}{2}\right|^2 d\omega\right\} \tag{14}$$

$$\hat{u}_k^{n+1}(\omega)=\frac{\hat{s}(\omega)-\sum_{i=1,i\neq k}^{K}\hat{u}(\omega)+\frac{\hat{\lambda}(\omega)}{2}}{1+2\alpha(\omega-\omega_k)^2} \tag{15}$$

$$\omega_k^{n+1}=\frac{\int_0^\infty\omega\left|\hat{u}_k(\omega)\right|^2 d\omega}{\int_0^\infty\left|\hat{u}_k(\omega)\right|^2 d\omega} \tag{16}$$

5. Repeat steps [2.] through [4.]. Stop the loop until (18) is satisfied.

$$\sum_{k=1}^{K} \frac{\left\| \hat{u}_k^{n+1} - \hat{u}_k^n \right\|^2}{\left\| \hat{u}_k^n \right\|^2} < \varepsilon \tag{18}$$

6. Perform inverse Fourier transform of $\hat{u}_k(\omega)$ to obtain the time domain form $\hat{u}_k(t)$.

D. TIME-FREQUENCY INFORMATION

Vital signs can be obtained after preprocessing and VMD processing. Time-frequency information of vital signs is presented from the Hilbert spectrum because it can describe the change rule of the data sequence in real time. In this way, we can procure the heartbeat and respiratory status in real time.

$$Z(t) = u_k(t) + j\tilde{u}_k(t) = a_k(t) e^{j\theta_k t} \tag{19}$$

$$a_k(t) = \sqrt{u_k^2(t) + j\tilde{u}_k^2(t)} \tag{20}$$

$$\theta_k(t) = \arctan \frac{\tilde{u}_k(t)}{u_k(t)} \tag{21}$$

Instantaneous frequency:

$$\omega_k(t) = \frac{d\theta_k(t)}{dt} \tag{22}$$

$Z(t)$ is the complex sequence and $\tilde{u}_k(t)$ is the Hilbert transform of $u_k(t)$. So echo signals can be represented as(23):

$$s(t) = Re \sum_{k=1}^{n} a_k(t) e^{j\int \omega_k(t)dt} \tag{23}$$

Because $a_k(t)$ and $\omega_k(t)$ are the functions of time, the Hilbert spectrum can describe changes in time domain.

III. THE DETECTION EXPERIMENT AND RESULT ANALYSIS

A. THE DETECTION EXPERIMENT

In the experiment, the PulsOn 440 Monostatic Radar Module (P440-MRM) was used to transmit and receive signals. P440-MRM is a portable UWB radar sensor. In order to improve the coupling noise phenomenon in the echo signals, broadband planar quasi Yagi antennas replaced original type omnidirectional dipole antennas in the measurement. The group delay of broadband planar quasi Yagi antennas is not more than 0.82ns. The antennas have good directivity and wide frequency band. The main parameters of broadband planar quasi Yagi antennas are shown in TABLE 1.

TABLE 1. Technical parameters of antennas.

Parameters	Values
Working Band	2.9GHz 10.1GHz
Polarization Mode	Linear polarized
Group Delay	$\leq 0.82ns$
Efficiency	usually>90%, minimum>71%
Gain	5-7dB

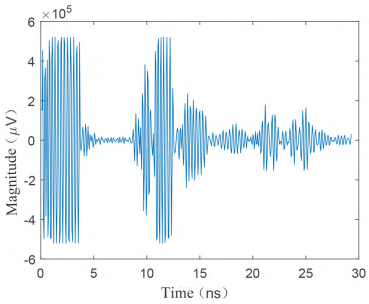

FIGURE 5. The omnidirectional dipole antenna.

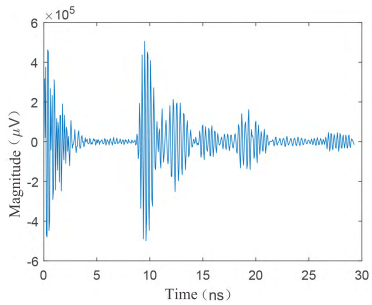

FIGURE 6. The broadband planar quasi yagi antenna.

Broadband planar quasi Yagi antennas can effectively reduce the coupling noise of echo signals compared with original type omnidirectional dipole antennas. As shown in the FIGURE 5 and FIGURE 6, coupling noise of broadband planar quasi Yagi antennas starts to decrease at 2 ns, while the coupling noise of original omni-dipole antennas begins to decrease at 4 ns. Echo signals begin to appear a large amount of information around 9ns because of the use of 1m SMA coaxial cable.

Next we set the important parameters in the experiment. Because the human respiratory rate is around 0.3hz and the heartbeat frequency is around 1Hz, the scan interval is set as 80 milliseconds according to Nyquist sampling law. The parameters of VMD algorithm are set as the TABLE 2.

TABLE 2. Parameters of VMD algorithms.

Parameters	Values
K, the number of intrinsic modes	4
τ, dual ascending step length	0
DC	1
$Init$, initializing the center frequency	0
ε, condition of convergence	10^{-5}
α, the convergence rate	2500

Processing the collected echo signals using preprocessing and VMD algorithm, the respiratory and heartbeat signals can be obtained.

B. RESULT ANALYSIS

We conducted two types experiments in total. The experimental results for human target detection without obstacle has been demonstrated. Futhermore, the experiment for human target who is behind concrete wall has been conducted as well.

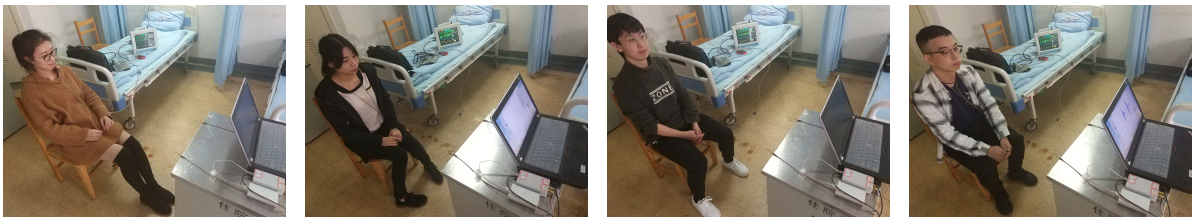

(a) (b) (c) (d)

FIGURE 7. The experiment for human body without obstacle. (a) Lady 1. (b) Lady 2. (c) Man 1. (d) Man 2.

1) EXPERIMENT WITHOUT OBSTACLE

The experiment conducted 481 scans via the P440-MRM. As the FIGURE 7 shows, the experiment to detect vital signs was carried out in the hospital of the University of Electronic Science and Technology. In this type of experiment, we have tested 4 people in total. 2 were ladies around 24 years old and the others were men of 24 years old. The distance of the antennas from the measured human body is important to the experimental results. In this type of experiment, we chose three distances to do the experiment. The three distance values are 0.65m, 0.80m, 0.95m. The experimental results of these three distances are shown in FIGURE 8.

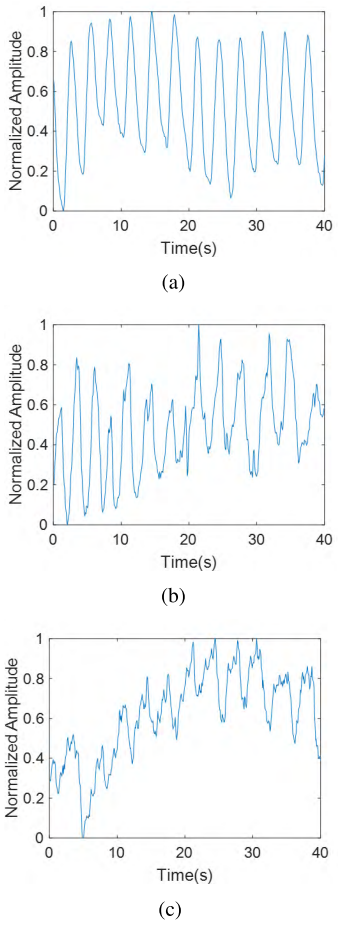

FIGURE 8. The time domain waveform without obstacle. (a) Distance = 0.65m. (b) Distance = 0.80m. (c) Distance = 0.95m.

It can be seen that chest movements in the time domain are clearly displayed. However, the time domain maps of the three distances are very different. When the distance is 0.65m and 0.80m, the breathing movements presented are very rugular. When the distance is 0.95m, the system based on UWB radar sensor cannot accurately obtain the law of respiratory movements. When the distance is 0.65m, it is too close to detect information of heartbeat. Because respiratory signals are too strong and heartbeat signals are too weak. So we decided choose distance as 0.80m. Although the movement of the breath can be clearly seen, the heartbeat movement cannot be displayed from the time domain map. Therefore we used the VMD algorithm to extract the respiratory signal and the heartbeat signal separately.

Due to the method, we successfully seperate respiratory and heartbeat signals. As the FIGURE 9 and 10 show, they are the frequency domain of two vital signs. We find the point where the normalization amplitude is 1 in FIGURE 9 and 10. The abscissa of this point is the respiratory or heartbeat frequency. To verify the accuracy of our experiment, we have to compare the results with ECG.

The next content is the statistical results of the two vital signs.

TABLE 3. Respiratory rates and heartbeat frequencys based on P440-MRM.

Target	Respiratory frequency(Hz)	Heartbeat frequency(Hz)
1(Lady 1)	0.3906	1.001
2(Lady 2)	0.2930	1.196
3(Man 1)	0.3662	1.221
4(Man 2)	0.3418	0.9521

The TABLE 3 represents the respiratory frequency and heartbeat frequency based on P440-MRM. Converting the frequency in the TABLE 3 to the number of times per minute and comparing it to ECG to acquire errors.

The TABLE 4 show the correct detection rates of respiratory and heartbeat according to the test results of comparison between P440-MRM and ECG. The correct rates of breath detection for person 1,3 and 4 are 100%. The correct rate for person 2 is 95%. These results indicate that the detection precision of the human body's respiratory with the method proposed in this paper is highly accurate. As the TABLE 4 shows, the correct rates of heartbeat detection for person1,2,3 and 4 correspond to 89%,90%,91%,87%. Even though they are not as high as the rates of respiratory, they still indicates

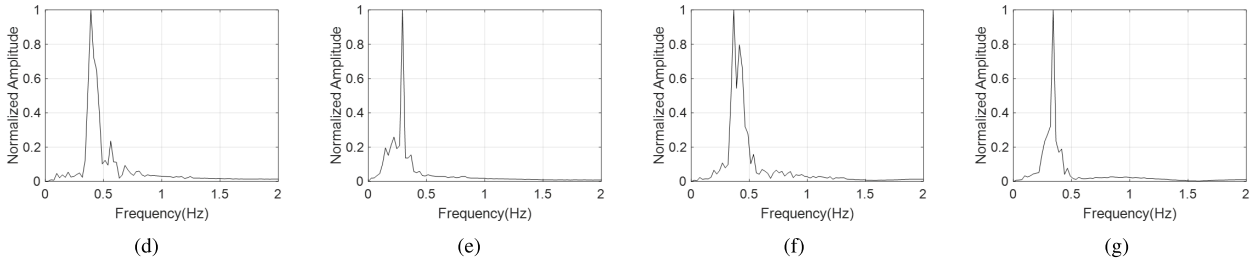

FIGURE 9. The respiratory rate. (a) Lady 1. (b) Lady 2. (c) Man 1. (d) Man 2.

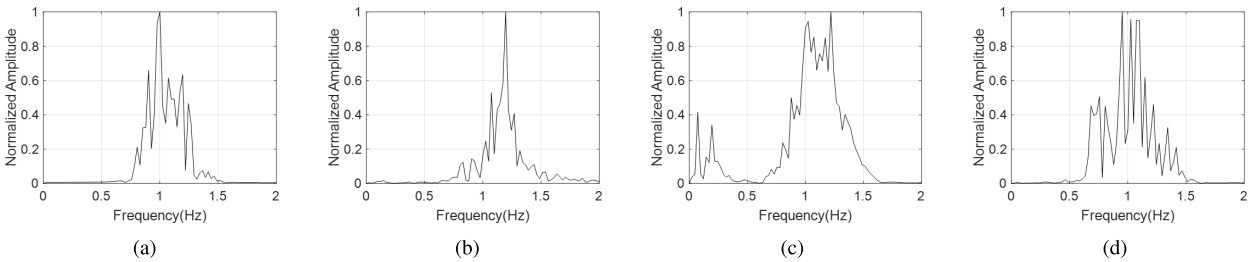

FIGURE 10. The heartbeat rate. (a) Lady 1. (b) Lady 2. (c) Man 1. (d) Man 2.

TABLE 4. Respiratory and heartbeat detection correct rates based on P440-MRM.

Target	Respiratory Detetction Correct Rates	Heartbeat Detetction Correct Rates
1(Lady 1)	100%	89%
2(Lady 2)	95%	90%
3(Man 1)	100%	91%
4(Man 2)	100%	87%

the frequency of heartbeat characteristics to a certain extent. When the target cannot be directly detected by touch, it is useful to detect using methods proposed in this paper.

In order to obtain time-frequency information, we also conduct the Hilbert transform. FIGURE 11 is a typical representative.

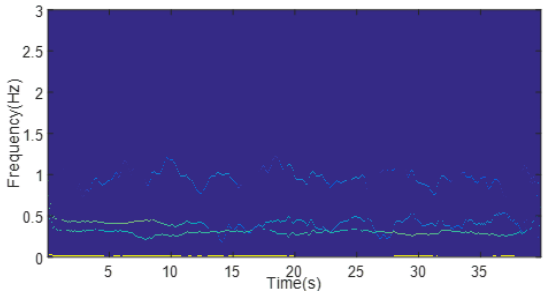

FIGURE 11. Time-frequency information.

From the FIGURE 11, time-frequency information of respiratory and heartbeat is well demonstrated. In some detection for patients, doctors need to know the patients' real-time breathing and heartbeat to diagnose the disease and the work done in this article provides a solution to this situation. As can be seen from the figure, the characteristics of breathing and heartbeat are well separated.

2) EXPERIMENT THROUGH-THE-WALL

The UWB radar sensor can penetrate non-matallic walls and obstacles, and identify the through wall human status [25]. In another type of test, we detect the human target behind concrete wall to make the method proposed in this paper have more practicality. The thickness of the wall is about 25 centimeters. From the results of the first type detection in this paper, we can draw that detection of respiratory based on the UWB radar sensor is reliable.And the detection through-the-wall is difficult to achieve in the hospital. For these reasons, we only did detection based on P440-MRM in this type of test, which is shown in FIGURE 12.

FIGURE 12. Experiment of target behind the wall.

FIGURE 13 gives the respiratory frequency which is 0.2808Hz. It is equivalent to 17 times per mimute. This can verify the study proposed in this paper is useful for rescue. When people are in ruins, the respiratory characteritics of those who need to be rescued can be obtained using methods

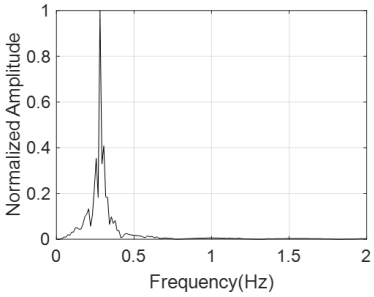

FIGURE 13. The Respiratory rate of target behind the wall.

we have proposed. This is very useful in improving rescue efficiency.

IV. CONCLUSION

In this paper, the respiratory and the heartbeat motions are detected clearly in the same test via the UWB radar sensor. These detections are reliable because they are very accurate. The correct detection rate of respiratory is over 95%, while the correct detection rate of heartbeat is around 90%. The detection system we designed contains P440-MRM and broadband planar quasi Yagi antennas and other equipments. The use of broadband planar quasi Yagi antennas can reduce the echo signals' coupling noise effectively. Hilbert spectra show the time-frequency information of vital signs detected by the UWB radar sensor. The result of detection through-the-wall demonstrates the great pratical significance of methods we put forward. When there is an obstacle between the perseon and the UWB radar sensor, the vital signs can still be obtained by the methods used in this paper.

The non-contact detection of vital signs via a UWB radar sensor is verified in this paper. Detection for multiple human bodies can be conducted in the future due to the superiority of the UWB radar signal. What's more, we can use networking technology to improve detection accuracy.

REFERENCES

[1] J. H. Reed, *Introduction to Ultra Wideband Communication Systems*. Upper Saddle River, NJ, USA: Prentice-Hall, 2005.

[2] P. Withington, H. Fluhler, and S. Nag, "Enhancing homeland security with advanced UWB sensors," *IEEE Microw. Mag.*, vol. 4, no. 3, pp. 51–58, Sep. 2003.

[3] M. Y. W. Chia, S. W. Leong, C. K. Sim, and K. M. Chan, "Through-wall UWB radar operating within FCC's mask for sensing heart beat and breathing rate," in *Proc. Eur. Radar Conf.*, Oct. 2005, pp. 267–270.

[4] Y. Pinhasi, A. Yahalom, and S. Petnev, "Propagation of ultra wide-band signals in lossy dispersive media," in *Proc. IEEE Int. Conf. Microw. Commun. Antennas Electron. Syst.*, May 2008, pp. 1–10.

[5] A. Muqaibel, A. Safaai-Jazi, A. Bayram, A. M. Attiya, and S. M. Riad, "Ultrawideband through-the-wall propagation," *IEE Proc.-Microw. Antennas Propag.*, vol. 152, no. 6, pp. 581–588, Dec. 2005.

[6] C. Li, J. Cummings, J. Lam, E. Graves, and W. Wu, "Radar remote monitoring of vital signs," *IEEE Microw. Mag.*, vol. 10, no. 1, pp. 47–56, Feb. 2009.

[7] L. Scalise, "Wireless sensing for the respiratory activity of human beings: Measurements and wide-band numerical analysis," *Int. J. Antennas Propag.*, vol. 2013, no. 3, Mar. 2013, Art. no. 396459.

[8] E. J. D. S. Luz, W. R. Schwartz, G. Cámara-Chávez, and D. Menotti, "ECG-based heartbeat classification for arrhythmia detection: A survey," *Comput. Methods Programs Biomed.*, vol. 127, pp. 144–164, Apr. 2016.

[9] S. Kiranyaz, T. Ince, and M. Gabbouj, "Real-time patient-specific ECG classification by 1-D convolutional neural networks," *IEEE Trans. Biomed. Eng.*, vol. 63, no. 3, pp. 664–675, Mar. 2016.

[10] T. Sharma and K. K. Sharma, "QRS complex detection in ECG signals using the synchrosqueezed wavelet transform," *IETE J. Res.*, vol. 62, no. 6, pp. 885–892, Sep. 2016.

[11] A. Page, O. Kocabas, T. Soyata, M. Aktas, and J.-P. Couderc, "Cloud-based privacy-preserving remote ECG monitoring and surveillance," *Ann. Noninvasive Electrocardiol.*, vol. 20, no. 4, pp. 328–337, Jul. 2015.

[12] E. M. Staderini, "UWB radars in medicine," *IEEE Aerosp. Electron. Syst. Mag.*, vol. 17, no. 1, pp. 13–18, Jan. 2002.

[13] I. Immoreev and T.-H. Tao, "UWB radar for patient monitoring," *IEEE Aerosp. Electron. Syst. Mag.*, vol. 23, no. 11, pp. 11–18, Nov. 2008.

[14] E. G. Ziganshin, M. A. Numerov, and S. A. Vygolov, "UWB baby monitor," in *Proc. 5th Int. Conf. Ultrawideband Ultrashort Impulse Signals*, Sep. 2010, pp. 159–161.

[15] A. Kumar, Q. Liang, Z. Li, B. Zhang, and X. Wu, "Experimental study of through-wall human being detection using ultra-wideband (UWB) radar," in *Proc. IEEE Globecom Workshops*, Dec. 2012, pp. 1455–1459.

[16] D. Zito, D. Pepe, B. Neri, F. Zito, R. D. De Ross, and A. Lanatà, "Feasibility study and design of a wearable system-on-a-chip pulse radar for contactless cardiopulmonary monitoring," *Int. J. Telemed. Appl.*, vol. 4, p. 328597, Jan. 2008.

[17] M. Mincica, D. Pepe, A. Tognetti, A. Lanatà, D. de Rossi, and D. Zito, "Enabling technology for heart health wireless assistance," in *Proc. IEEE Int. Conf. e-Health Netw. Appl. Services*, Jul. 2010, pp. 36–42.

[18] D. Zito, D. Pepe, M. Mincica, and F. Zito, "A 90 nm CMOS SoC UWB pulse radar for respiratory rate monitoring," in *IEEE ISSCC Dig. Tech. Papers*, Feb. 2011, pp. 40–41.

[19] F. Michahelles, R. Wicki, and B. Schiele, "Less contact: Heart-rate detection without even touching the user," in *Proc. 8th Int. Symp. Wearable Comput.*, vol. 1, Oct./Nov. 2004, pp. 4–7.

[20] C.-P. Lai, Q. Ruan, and R. M. Narayanan, "Hilbert-Huang transform (HHT) analysis of human activities using through-wall noise radar," in *Proc. Int. Symp. Signals Syst. Electron.*, Jul./Aug. 2007, pp. 115–118.

[21] X. Zhang and Z. Zhang, "Near-field plate applied in wireless power transmission system," *J. Tianjin Normal Univ.*, vol. 37, no. 6, pp. 58–61, 2017.

[22] S. Ma and Y. Wang, "Design and implementation of an ultra-wideband high-accuracy ranging system," *J. Tianjin Normal Univ.*, vol. 37, no. 6, pp. 55–57, 2017.

[23] M. Shi and X. Gong, "Parameters identification method via cepstrum analysis for mix blurred image restoration," *J. Tianjin Normal Univ.*, vol. 37, no. 5, pp. 60–65, 2017.

[24] K. Dragomiretskiy and D. Zosso, *Variational Mode Decomposition*. Piscataway, NJ, USA: IEEE Press, 2014.

[25] W. Wang, Y. Jiang, and D. Wang, "Through wall human detection based on stacked denoising autoencoder algorithm," *J. Tianjin Normal Univ.*, vol. 37, no. 5, pp. 50–54, 2017.

ZHENZHEN DUAN received the B.S. degree from the University of Electronic Science and Technology of China, in 2016, where she is currently pursuing the M.S. degree with the Department of Information and Communication Engineering. Her research interests include ultra-wideband radar for human detection and clutter suppression.

JING LIANG received the B.S. and M.S. degrees in electrical engineering from the Beijing University of Posts and Telecommunications, Beijing, China, in 2003 and 2006, respectively, and the Ph.D. degree in electrical engineering from the University of Texas at Arlington, in 2009. She is currently an Associate Professor with the Department of Electronic Engineering, University of Electronic Science and Technology of China. Her current research interests include radar sensor networks, collaborative and distributed signal processing, wireless communications, compressive sensing, wireless networks, and fuzzy logic systems.